Fast geometric factor approximation to evaluate the electrical resistivity of concrete and reinforced concrete specimens using neural network models

Wael Karam [1*], *Yann* Lecieux[1], *Mathilde* Chevreuil[1], and *Franck* Schoefs[2]

[1]Nantes Université, Ecole Centrale Nantes, CNRS, GeM, UMR 6183, F-44000 Nantes, France
[2]Nantes Université, ISOMer, UR 2160, F-44000 Nantes, France

Abstract. The measurement of electrical resistivity has applications in civil engineering, particularly in condition assessment, structural health monitoring, and material characterization. Accurately evaluating material resistivity requires determining a geometric factor, which depends on specimen geometry, electrode positioning, and the presence of reinforcement. Several methods exist for calculating this factor, including numerical modelling and experimental approaches. This study presents an approximation technique using surrogate models to rapidly calculate geometric factors for non-reinforced and reinforced geometries. The studied geometries are prismatic, with the reinforced case involving a single embedded bar, commonly used in laboratory studies. These surrogate models are based on neural networks trained with data generated through finite element modelling. The results are validated against literature data, including studies by Minagawa et al. (2023) [1] and Presuel-Moreno et al. (2013) [2]. This research provides a generalized method for evaluating geometric factors and serves as a proof of concept that this approach can effectively approximate them. It accelerates resistivity data processing and facilitates parametric analyses. Additionally, it complements previous studies, which were limited to the central positioning of measurement devices, by enabling the evaluation of geometric factors across a wider range of specimen dimensions and measurement positions on the surface of the domain. As an initial study, it lays the foundation for applying this method to other geometries in future work.

1 Introduction

DC-electrical resistivity measurements have been applied to concrete for several decades [3,4], mainly due to their sensitivity to moisture content and chloride concentration in the pore solution of concrete [5,6], which are key parameters for evaluating the durability of concrete structures. These resistivity measurements can also serve as relevant indicators of mechanical strength [7], crack presence [8] and the corrosion state of reinforcing bars [9]. The data obtained during an electrical resistivity measurement campaign include the values of the injected electric current I and the measured potential differences ΔV. From these measured data, the electric resistance is derived as defined by Ohm's law $R = \Delta V / I$. The value of R depends on the geometry and does not directly provide access to the resistivity of the probed medium [10]. Considering the geometry of the probed medium and any factors influencing the measurements, such as the presence of reinforcement bars, is necessary to accurately deduce the resistivities from these measurements, by estimating the corresponding geometric factors K as precisely as possible. Several studies have been conducted to determine the geometric factors K for specific specimen sizes when using the four-point measurement. For example, Morris et al. [11] addressed the case of standard-sized cylinders used in compressive strength and rapid chloride permeability tests, providing both experimental and modelling-based geometric factors. Similarly, Minagawa et al. [1] presented a study that calculated appropriate geometric factors for various concrete specimens typically used in laboratories (prismatic and cylindrical shapes) and discussed the effects of probe spacing and specimen dimensions on measurement results. Furthermore, several studies have shown that resistivity measurements are disturbed in the presence of steel reinforcements [12–14], and the apparent resistivity significantly decreases due to the high conductivity of steel [15,16]. Hence, numerous approaches have been proposed to account for the presence of steel bars or to minimize their effect on the measurement. One of these approaches involves placing the electrodes at a certain distance diagonally from the rebars within the rebar mesh [3]. Another approach consists of creating a model that describes the presence of reinforcement and its short-circuit effect by considering the electrochemical state of the steel [15,17,18]. Two other studies, conducted by Garzon et al. [16] and by Samson et al. [19], introduce a 'rebar factor' into the apparent resistivity formula to mitigate the rebar effect, specifically focusing on

* Corresponding author: wael.karam@univ-nantes.fr

particular slab geometries and concrete with homogeneous resistivity. Despite these numerous studies, there is still a lack of generalization in the calculation of geometric factors for specimens of known shapes with any specified dimensions and electrodes positions. This generalization is important for studying the spatial variability of resistivity caused by the variability of the material of the medium being probed. The first objective of this work is to assess the relevance of approximation models for predicting geometric factors for a wide range of configurations.

Based on the results of the approximation models, the second objective is to complement previous studies [1,2,16], which were limited to the central positioning of measurement devices, by enabling the evaluation of the geometric factor across a wider range of specimen dimensions and for any positioning of the measurement device on the surface of the domain.

Thus, geometric factors are calculated within the framework of surface measurement with four-probe devices on cuboid shapes, with or without rebars, employing neural network models. Furthermore, the study focuses on the following points:

- detailing the steps for data generation and constructing approximation models to predict the geometric factor needed for resistivity measurement analysis within cuboid shapes used for laboratory study without reinforcement, using four-probe surface measurements;
- constructing an approximation model for reinforced cuboid specimens with a single bar in x direction;
- verifying the results against those published in the literature, particularly in the articles by Minagawa et al.(2023) [1] and Presuel-Moreno et al. (2013) [2];
- Illustrating the combined effect of the boundaries and the conductive elements on resistivity measurements.

Section 2 of this paper provides a brief overview of the DC-electrical method, its measurement principles, and various approaches for evaluating geometric factors. Section 3 constitutes the core of the analysis, offering an exhaustive exposition of the proposed approaches based on surrogate models. This includes the modeled geometries, data generation, and the approximation models used. The Results section presents the uncertainty quantification of the created models, followed by the verification of results, and concludes with perspectives and conclusions.

2 Principal of DC- electrical method and the evaluation of the geometric factor

The DC-electrical method is a non-destructive testing technique that utilizes direct current (DC) to measure the electrical resistivity of the probed domain. In the fields of structural diagnosis and material characterization, various devices are employed to assess the electrical resistivity of concrete [20]. One such device, the uniaxial measurement device [10], consists of two parallel plates that serve as both injection and potential measurement electrodes. Alternatively, separate measurement electrodes [21], such as additional plates

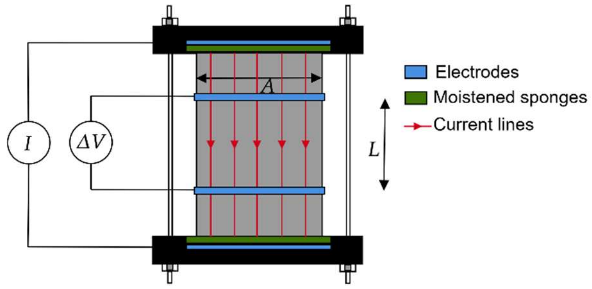

Fig. 1. Uniaxial measurement device

or rings in contact with the specimen (Fig. 1), can be used to minimize measurement errors. This measurement configuration allows for the analytical evaluation of the geometric factor and, consequently, the bulk resistivity ρ of concrete by the direct application of Ohm's law, as indicated by equation 1:

$$\rho = K\frac{\Delta V}{I} \quad (1)$$

With K=S/L is the geometric factor, S is the cross-sectional area of the cylinder, L is the distance between measuring electrodes, ΔV is the measured potential difference (in Volt), and I is the intensity of the injected current in ampere.

The other type of resistivity device consists of four aligned electrodes (Fig. 2). Two electrodes, labeled A and B inject the electric current I, while the other two, M and N, are used to measure the electric potential difference ΔV [22]. This type of device is the most commonly used for on-site investigations (e.g., Proceq® Resipod device).

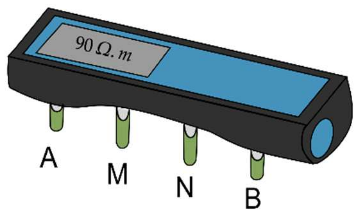

Fig. 2. Four electrode devices consisting of two injection electrodes labeled A and B and two measurement electrodes labelled M and N

Using the same principle, devices with multiple aligned electrodes can be used to generate a tomography of the investigated medium [23,24]. For these types of measurements, the geometric factor has an analytical expression in specific cases, such as a semi-infinite medium. Therefore, equation 2 provides its expression for this scenario [25]:

$$K = \frac{2\pi}{\frac{1}{AM} - \frac{1}{AN} - \frac{1}{BM} + \frac{1}{BN}} \quad (2)$$

If the configuration Wenner-α ($i.e, AM = MN = NB = s$) is used, then the geometric factor simplifies to 2πs. This expression is not applicable in cases involving finite specimens, proximity to boundaries, or conductive elements (e.g., steel reinforcement). Thus, in such cases, the geometric factor can be evaluated using experimental or modelling approaches [26]. The experimental approach consists of reproducing the same geometry as the investigated medium using a homogeneous material of known resistivity (ρ_{ho}), such as water. For each measurement, an electric current I_{inj} is injected into the medium, and a potential difference ΔV_{mes} is measured. The corresponding geometric factor is then given by equation 3 [26]:

$$K = \rho_{hom} \frac{I_{inj}}{\Delta V_{mes}} \quad (3)$$

The accuracy of this method depends on the ability to replicate the geometry precisely and on the precision of the measurement devices.

The numerical modelling approach follows the same concept as the experimental method. It involves numerically reproducing the investigated medium using a finite element model. This is done by modelling the geometry with homogeneous resistivity while considering boundary conditions and the presence of conductive elements, such as reinforcement. A current is injected, and the potential difference is computed by solving Poisson's equation (see equation 4), which describes the diffusion of electric current within the medium:

$$\vec{\nabla}.\left(-\frac{1}{\rho}\vec{\nabla}V\right) + \delta_A I - \delta_B I = 0 \quad (4)$$

Where $-\delta_A I$ and $\delta_B I$ are point current sources of intensity I, imposed by electrodes placed at points A and B, respectively.

Once the potential difference is calculated, the geometric factor is determined using equation 3.

This study uses the numerical approach to generate a geometric factor database for reinforced and non-reinforced specimens.

3 Fast evaluation of geometric factors: modeled geometries, generated data and approximation models

In cases where the spatial variability of the material needs to be studied, evaluating the geometric factor for a large number of measurement point on the surface is essential. However, creating a finite element model or an experimental model for each measurement to assess the geometric factor is tedious. To overcome this limitation, two test cases, including reinforced and non-reinforced prismatic specimens, were modeled using the finite element method to cover most of typical specimen dimensions used in laboratory experiments. An automated mesh generation process was implemented to generate the data: Matlab controls the Gmsh software [27] used to create the geometry and mesh. Once generated, these are imported into Matlab, where the Poisson equation is solved and the geometric factor is evaluated. The specimen is discretized using a fine mesh near the electrodes, with a size of $\boldsymbol{Smin/8}$ where $\boldsymbol{Smin}$ is the distance between two probes. The size of the elements is gradually expanding to reach $\boldsymbol{3.Smin/8}$ at the bottom of the domain. Boundary conditions include injecting a point current (I=±1A) at the positions of electrodes A and B and imposing a zero potential (V=0) at a specified point of the geometry to guarantee the unicity of the solution. The medium is assumed to be homogeneous, with a constant resistivity of 100 **Ω**·m, typical of concrete inspection scenarios.

3.1 The adopted modelling hypothesis

Several modelling hypotheses were adopted in this study:

1- The electrodes are treated as point sources and placed on the medium's surface.
2- The electrodes' configuration is Wenner.
3- The concrete domain is considered purely conductive and homogeneous (non-polarizing).
4- The steel rebars are considered extremely conductive elements with perfect contact with the concrete. Thus, no polarization phenomena or changes in the electrochemical state of the steel-concrete interface are taken into account in this paper

3.2 The modeled geometries and the generated data

3.2.1 Case of homogeneous non-reinforced cuboid-type specimens (case a)

In this study, the first case analyzed (case a) involves a cuboid geometry, one of the common shapes used for electrical resistivity measurements with four-probe devices on non-reinforced concrete specimens. Previous research, including work by Minagawa et al. [1], has developed models to determine geometric factors for this shape. However, these studies were limited to central measurements. This study complements Minagawa's work by considering a cuboid geometry that allows measurements to be taken at various positions on the surface of the domain. The factors influencing the geometric factor for case a) include the domain dimensions and the positions of the electrodes. The domain dimensions are selected within the following range:

- $L_x \in [8\ cm, 80\ cm]$: length in x direction
- $L_y \in [5\ cm, 40\ cm]$: width in y direction
- $L_z \in [4\ cm, 20\ cm]$: height in z direction

For each generated geometry, the positions of the four electrodes are chosen uniformly on a grid along the x and the y directions on the surface of the domain. The electrodes spacing range from $2\,cm$ to $14\,cm$ in a Wenner configuration ($AM = MN = NB = s$). It is important to note that electrodes can be positioned no closer than 1 cm from the free edges (see the blue dashed line in Fig. 3). A total of 120 different geometries were simulated to create a large dataset for approximating the geometric factor with a model with seven parameters $L_x, L_y, L_z, X_A, Y_A, X_B, Y_B$ where X_A, Y_A, X_B and Y_B are the coordinates of injection electrodes A and B.

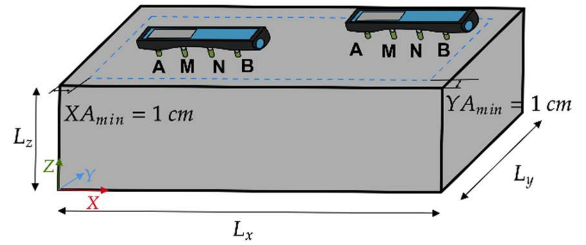

Fig. 3. Illustration of the prismatic modelled geometry (case a), showing the measurement devices and the limits within which the measurements can be taken (see blue dashed lines).

3.2.2 Case of reinforced cuboid specimens with a single bar in x direction (case b)

The proposed reinforced case in this study takes the form of a cuboid reinforced with a single bar in the x-direction (Fig. 4.a). The steel bar is positioned at the center of the specimen, such that the bar axis is located at $Y = Ly/2$, where L_y is the dimension of the specimen in the y-direction (Fig. 4b). This bar is spaced from the surface and from the two faces normal to the x-direction by a distance c (the cover thickness). The steel bar is modeled using cylindrical conductive bars with a resistivity of $10^{-8}\,\Omega \cdot m$ while the surrounding domain has a resistivity of $100\,\Omega \cdot m$.

Nine parameters influence the geometric factor calculation, as shown in Fig. 4: the dimensions of the probed domains (Lx, Ly, Lz), the positions of the electrodes defined by the coordinates of electrodes A and (XA, YA, XB, YB), the radius of the reinforcement bar (r), and the thickness of the concrete cover (c). The ranges of these parameters are uniformly generated as follows:

- the electrodes spacing $s \in [2\,cm, 14 cm]$
- the cover thickness $c \in [2.5\,cm, 7.5\,cm]$
- the rebar radius $r \in [0.3\,cm, 1\,cm]$
- $L_x \in [20\,cm, 80\,cm]$: length in x direction
- $L_y \in [5\,cm, 40\,cm]$: width in y direction
- $L_z \in [4\,cm, 20\,cm]$: height in z direction
- For the parameters (X_A, Y_A, X_B, Y_B), the electrodes can be positioned at any position on the surface while the closest distance to the surface boundary is 1 cm (see the blue dashed line in Fig. 4.a).

A total of 120 different reinforced geometries, spanning the parameter ranges defined previously, were simulated to create a large dataset for approximating the geometric factor.

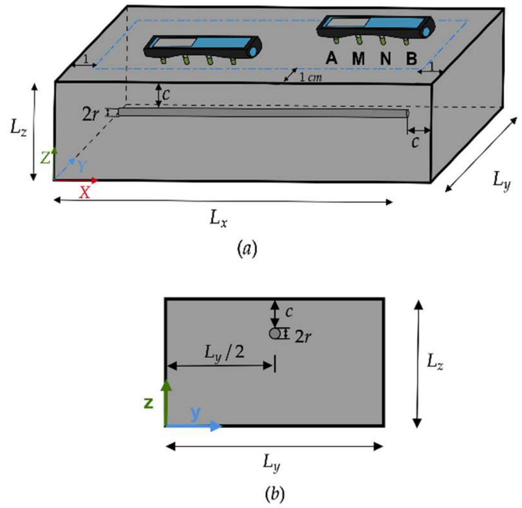

Fig. 4. a) Illustration of the modelled cuboid geometry with a single reinforcement bar (case b). **b)** The cross-sectional area in the x-z plane of the modelled geometry (case b), showing the position of the reinforcement bar.

3.3 The approximation model for the fast evaluation of the geometric factor

The creation of an approximation model that can predict the geometric factor for different reinforced and unreinforced shapes involves using models with several input factors and one output factor. Due to the complex nature of electric current flow in finite mediums and the geometric factor itself, a neural network model is selected. A basic neural network usually has an input layer, one or more hidden layers, and an output layer (see Fig. 5). Weights and biases link neurons in these layers. When a neural network has just one hidden layer, it is called a simple artificial neural network. Conversely, networks with several hidden layers are known as Deep Neural Networks (DNN) [28]. This study uses deep neural network models based on the complexity of the specific geometries being studied. The neural networks for this research were trained using the Deep Learning Toolbox available in Matlab. Detailed information about each model created is given in the next section.

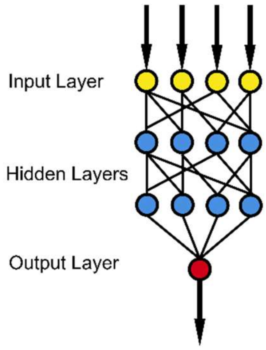

Fig. 5 Neural network structure.

4 Results

In this section, a neural network model is created for each specific geometry to quickly predict the geometric factor. As mentioned earlier, the data was generated through finite element models. For all the cases studied, the dataset is divided into three parts: the training set, which consists of 80% of the data and is used to train the neural network, a validation set of 10% that is used to adjust the model, and a test set of 10% to evaluate the model's predictive ability. The structure of the model, including the number of hidden layers and the number of neurons in each layer, is determined through a trial-and-error process to find the best configuration that minimizes error. The training effectiveness is assessed using the mean square error (MSE) between the outputs of the neural network and the actual results. This error is calculated for each iteration, or epoch, as the neural network learns from the dataset. The number of epochs plays an important role in finding an optimal neural network structure that provides the highest prediction accuracy. In this study, the training process is conducted over 1000 epochs. All the commonly chosen model settings are summarized in Table 1.

Table 1. Chosen Settings in Matlab's Neural Network Training function

NN Parameters	**Chosen Settings**
NN type	Feedforward Neural Network
Training Algorithm	Levenberg-Marquardt (trainlm)
Loss Function	Mean Squared Error (mse)
Hidden Layers and Neurons	specified for each case
Activation Functions	Linear
Data Division	80% training, 10% validation, 10% testing
Max Epochs	1000
Learning Rate	0.01
Initial Weights and Biase	Randomly initialized

4.1 Neural network model for cuboid homogeneous shape (case a)

As stated in section 3.2.1, the geometric factor K (output) for a homogeneous cuboid shape is influenced by seven key parameters defining the geometry of the domains and the positions of electrodes: $L_x, L_y, L_z, X_A, Y_A, X_B$ and Y_B. To estimate $K = f(L_x, L_y, L_z, X_A, Y_A, X_B, Y_B)$, the neural network model consists of two hidden layers comprising 50 and 25 neurons, respectively. The prediction capacity of the neural network is evaluated through error histograms (Fig. 6). These histograms display the relative difference $\boldsymbol{RE}$ between the predicted geometric factors K_{NN} and the values obtained from finite element K_{FE} (test sample). The components of $\boldsymbol{RE}$ are calculated as follows:

$$RE_i = \frac{K_{FE_i} - K_{NN_i}}{K_{FE_i}} \times 100 \tag{5}$$

with $i = 1, \dots, n$ where n denotes the length of the sample test vector. It can be observed that $\boldsymbol{RE}$ follows a symmetric distribution with low dispersion, characterized by a mean equal to -0.0013 % and a standard deviation of 0.2380 %. The second statistical parameter analyzed is the Mean Absolute Percentage Error ($MAPE$), defined as:

$$MAPE = \frac{1}{n}\sum_{i=1}^{n}\left|\frac{K_{FE_i} - K_{NN_i}}{K_{FE_i}}\right| \times 100 \tag{6}$$

In this case, the Mean Absolute Percentage Error (MAPE) is 0.15131 %, , indicating that the prediction errors from the neural networks are relatively small in comparison to other uncertainties associated with electrical resistivity measurements. Additionally, the regression graphs for the testing datasets are illustrated in Fig. 7. The correlation coefficient, denoted as R, between the predicted (K_{NN}) and reference (K_{FE}) geometric factor, is calculated using the following formula:

$$R = \frac{1}{n-1}\sum_{i=1}^{n}\left(\frac{K_{NN_i} - \mu_{K_{NN}}}{\sigma_{K_{NN}}}\right)\left(\frac{K_{FE_i} - \mu_{K_{FE}}}{\sigma_{K_{FE}}}\right) \tag{7}$$

where $\mu_{K_{NN}}$ and $\sigma_{K_{NN}}$ represent the mean and standard deviation of the geometric factors predicted by the neural network model on the test sample, while $\mu_{K_{FE}}$ and $\sigma_{K_{FE}}$ correspond to those computed using the finite element model. The high correlation coefficient $R = 0.99999$ demonstrates the strong predictive performance of the neural network model. This confirms that the deep neural network (DNN) approach can accurately predict the geometric factor for any position of the measurement quadripole on the surface of the examined medium.

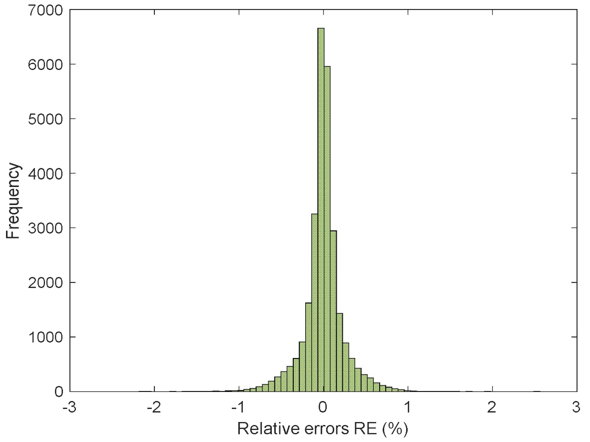

Fig. 6. Histogram showing the relative difference error RE between predicted and finite element geometric factors for case a.

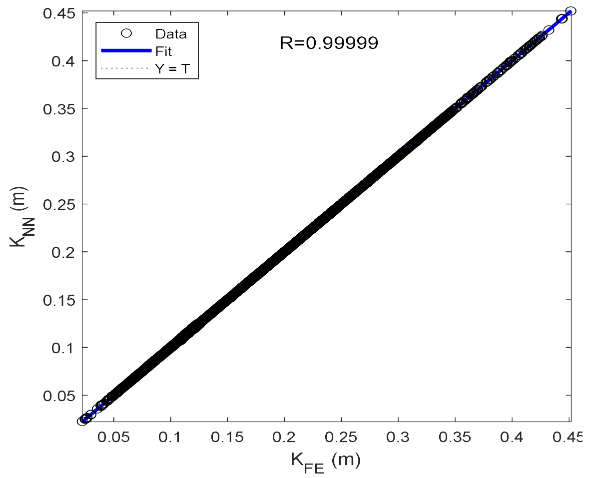

Fig. 7. Graph showing the correlation between the geometric factor K predicted by the NN model and finite element model for case a.

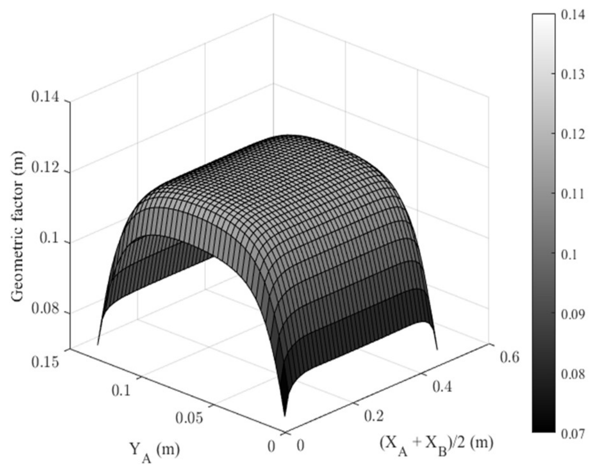

Fig. 8. A 3D surface representation of the geometric factor assessed using the proposed approximation model for a domain with dimensions $L_x = 53\ cm$, $L_y = 15\ cm$, and $L_z = 15\ cm$, for different quadripole ABMN positions, with a constant electrode spacing of 2 cm.

To further emphasize the influence of geometric effects on resistivity variability assessments, the approximation model was employed to calculate geometric factors for measurements taken on the surface of a medium with dimensions $L_x = 53\ cm$, $L_y = 15\ cm$, and $L_z = 15\ cm$, with fixed electrode spacing of 2 cm. The geometric factor is illustrated as a 3D surface according to the position of the quadripole center (Fig. 8). The results reveal that the geometric factor varies with electrode placement and is significantly influenced by boundaries, with a notable decrease as electrodes approach the edges. A marked decline occurs when the quadripole is near the corners. It is also noteworthy that, in the middle of the domain, the surface shape presents a level region of values approximately equal to the geometric factor in the semi-infinite medium, $(2\pi s)$. This variability highlights the importance of considering boundary effects, as overlooking them may lead to biases in resistivity assessments. The proposed approximation model offers an efficient method for rapidly evaluating the geometric factor across different geometries, electrode positions, and spacings, leading to a more precise analysis of resistivity variability in the studied area.

4.2 Validation of the neural network model using the literature data from Minagawa et al. (case a)

In 2023, Minagawa et al. [1] conducted a study on several prismatic specimens of varying sizes, commonly used in laboratory tests. The authors reported the geometric factors for surface measurements performed on these specimens, using centrally positioned electrode quadripoles aligned along the x-direction. The geometric factors were calculated through a finite element model, and the results presented by Minagawa et al. [1] were experimentally validated, demonstrating the reliability and practicality of their model. Additionally, they examined how probe spacing influences electrical resistivity measurements in the tested medium. Notably, Minagawa et al. [1] defined the geometric factor as the inverse of the traditional expression K. Specifically, the geometric factor is presented as $K_{Minagawa} = \rho.\Delta V/I$, expressed in (m^{-1}). In this subsection $K_{Minagawa}$ is plotted in its figures. To verify the neural network's accuracy, two of the specified geometries were selected:

- Volume 1: $L_x = 40$ cm, $L_y = 10$ cm, $L_z = 10$ cm
- Volume 2: $L_x = 53$ cm, $L_y = 15$ cm, $L_z = 15$ cm

The geometric factor was evaluated for various electrode spacings ranging from 2 cm to 9 cm. The geometric factors predicted by the neural network were compared with those given by Minagawa et al. [1], as shown in Fig. 9. The predicted values are very close to those in the original study. Additionally, Fig. 10 illustrates the relative error, expressed as a percentage, between the predicted geometric factors using the proposed neural network approach and the values from the article (see equation 5). Notably, the maximum error for both geometries is 0.57% in absolute value, indicating a high level of accuracy in the predictions made by the neural network model. The model consists of only 2 hidden layers, and its strong predictive performance suggests that the geometric factor data exhibits moderate complexity and non-linearity for the evaluated cuboid shape.

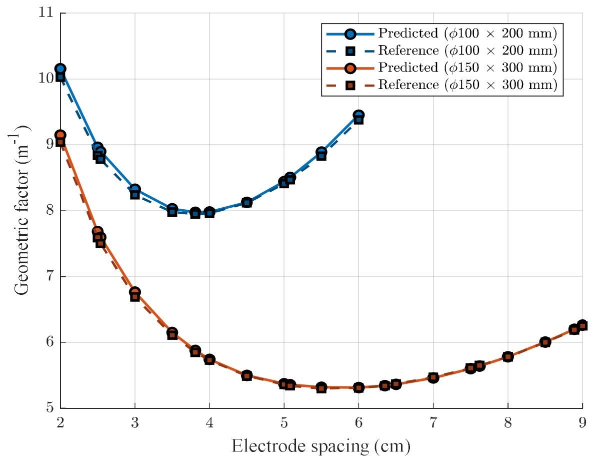

Fig. 9. Comparison of the geometric factors obtained from Minagawa et al. [1] and those predicted by the neural network model as a function of probe spacing for two cuboid geometries.

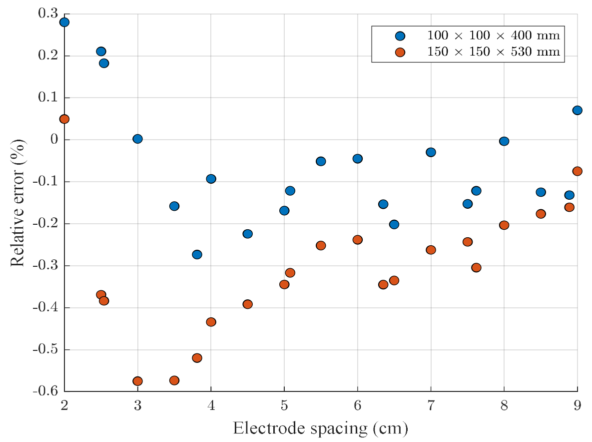

Fig. 10. Graphs depicting the relative error (%) between the geometric factor predicted by the NN model and the values from Minagawa et al.'s article [1] for a centered quadripole ABMN on two cuboid shapes.

4.3 Neural network model for reinforced cuboid specimens with a single bar in x direction (case b).

In addition to the seven parameters identified for the unreinforced cuboid shape, two more parameters influence the geometric factors of a cuboid reinforced with a single bar in the x-direction. As noted in section 3.2.2, these additional parameters include the cover thickness c, and the radius of the steel bar r. Due to the complex nature of the data, especially when measurements are taken near the steel bar (resulting in very high geometric factors), the output K is replaced by the napierian logarithm of K to reduce the non-linearity of data. Therefore, to estimate $log(K) = f(L_x, L_y, L_z, X_A, Y_A, X_B, Y_B, r, c)$, a neural network (NN) is utilized featuring two hidden layers with 50, 25 neurons respectively. Fig. 11 displays the histogram of $\boldsymbol{RE}$. It is notable that $\boldsymbol{RE}$ shows very low dispersion, with a standard deviation of 0.2222% and a mean of 0.0038 %. The MAPE value is 0.16059%.

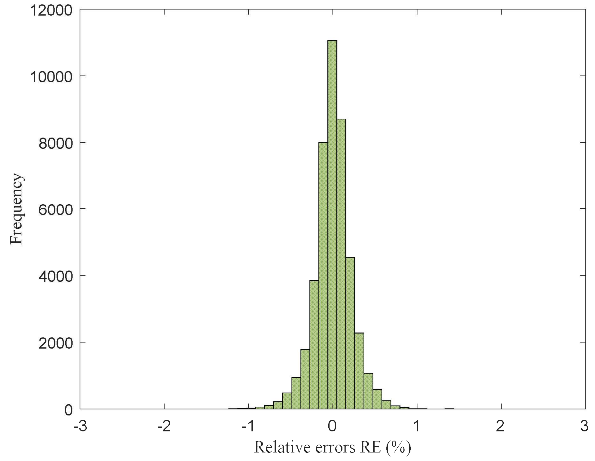

Fig. 11. Histogram showing the relative difference error RE between predicted and finite element geometric factors for case b.

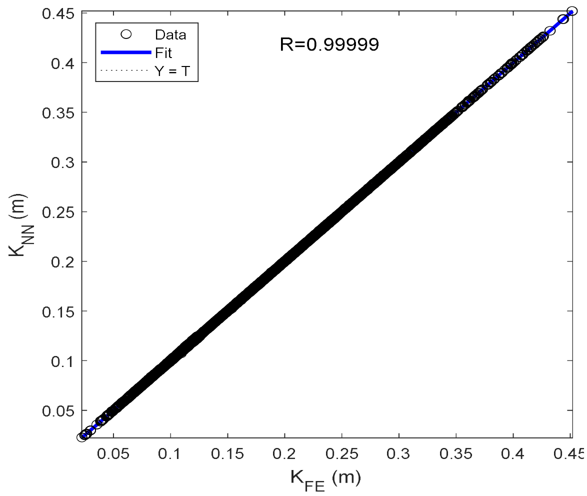

Fig. 12. Graph showing the correlation between the geometric factor K predicted by the NN model and finite element model for case b.

The regression graph in Fig.12 demonstrates the correlation between the modelled and predicted geometric factors from the test sample, indicating that the neural network model has strong predictive capability ($R = 0.99999$).

This neural network model provides a reliable and rapid assessment of the geometric factor. It can be useful for assessing the influence of conductive elements and boundary conditions on the resistivity measurement.

To achieve this and to compare the results with those presented in section 4.1 for an unreinforced prismatic geometry, the same geometry was considered with the following dimensions: $L_x = 53\ cm$, $L_y = 15\ cm$, and $L_z = 15\ cm$. A quadripole parallel to the reinforcement bar (in the x-direction) was used, with a fixed electrode spacing of 2 cm. Additionally, a steel bar with an 8 mm diameter was embedded in the medium, ensuring a cover thickness of 3 cm. For this configuration, a 3D surface of the evaluated geometric factor using the neural network (NN) is illustrated as a function of the quadripole center position (Fig. 13).

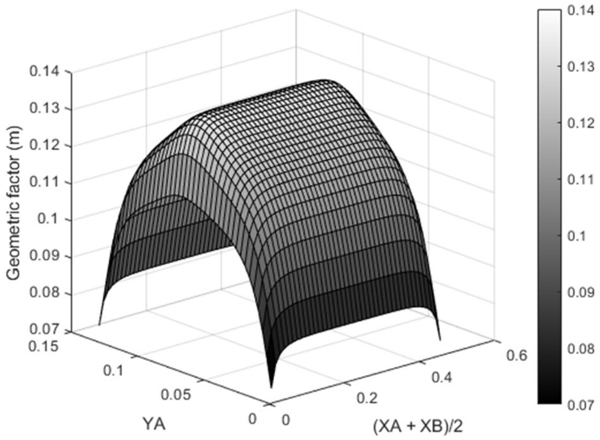

Fig. 13. A 3D surface representation of the geometric factor, evaluated using the proposed approximation model, for a centrally reinforced domain containing a single steel bar. The domain dimensions are $L_x = 53\ cm$, $L_y = 15\ cm$, and $L_z = 15\ cm$. The geometric factor is analyzed for different quadripole (ABMN) positions, with a constant electrode spacing of 2 cm.

The results reveal that the geometric factor varies with electrode placement and is significantly influenced by boundaries, showing a notable decrease as the electrodes approach the edges. A sharp decline is observed when the quadripole is near the corners. Furthermore, when comparing the surface profile with the non-reinforced case, it is evident that near the centrally placed reinforcement bar, the surface exhibits an increase with a steeper slope, reaching a maximum when measurements are taken directly above the reinforcement bar. These findings reaffirm that using the geometric factor calculated for a semi-infinite medium ($2\pi s$) is inaccurate in the presence of steel and near the boundaries. This underscores the importance of the proposed approximation approach, which effectively accounts for boundary and conductive element effects with accuracy without the need for new finite element modelling four each measurement position or geometry.

4.4 Validation of neural network models using literature data reported in Presuel-Moreno et al. 2013 (case b).

Presuel-Moreno et al. (2013) [2] conducted a numerical modelling study using the finite element method to examine how rebar presence, multilayered concrete resistivity, and their combined effects influence the apparent resistivity of concrete measured with the Wenner probe. The study considered various geometries, both with and without rebars. To validate the accuracy of the constructed neural network in predicting the geometric factor, the geometry and data from Presuel-Moreno were utilized, specifically focusing on a cuboid specimen containing a single rebar (Fig. 14.a). A 4-electrode array was simulated to take measurements at different positions (Fig. 14.b). The rebar had a diameter of 16 mm.

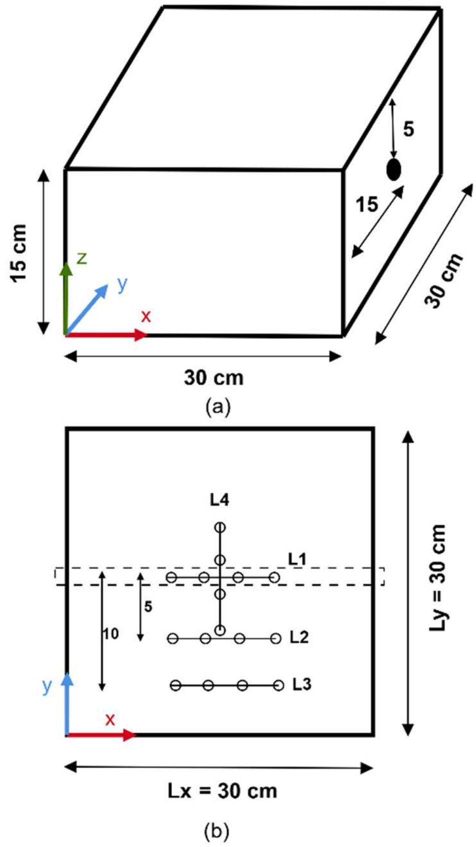

Fig. 14. a) 3D representation and **b)** XY plane view of the centrally reinforced domain containing a single steel bar, as presented in the article by Presuel-Moreno et al. (2013), illustrating different measurement positions.

Table 2. Comparative table of the predicted and reference geometric factors from the neural network model and the article by Presuel-Moreno et al. (2013), respectively.

Meas.	K_{ref}	K_{NN}	RE (%)
$(L1, s = 3cm)$	0.2005	0.1974	-1.55
$(L1, s = 5cm)$	0.3785	0.3678	-2.83
$(L2, s = 3cm)$	0.1904	0.1880	-1.26
$(L2, s = 5cm)$	0.3173	0.3099	-2.33
$(L3, s = 3cm)$	0.1762	0.1742	-1.14
$(L3, s = 5cm)$	0.2493	0.2455	-1.52
$(L4, s = 3cm)$	0.1848	0.1832	-0.87
$(L4, s = 5cm)$	0.2830	0.2807	-0.81

Table 2. summarizes the geometric factors provided by the study of Presuel-Moreno et al. (2013) [2], the predicted geometric factors using the neural network

model, and the relative differences between them for both 3 cm and 5 cm electrodes spacing (s). These comparisons are made for different electrodes positions and orientations ($L1, L2, L3$, and $L4$) as illustrated in Fig. 14.b.

For all the measurements (L1, L2, L3, and L4), the proposed neural network has accurately calculated the values of the geometric factors, as seen in the relative difference values between K_{NN} and K_{ref} (as given in [2]), with a maximum value of -2.83%. This modelling error is considered minimal compared to other sources of uncertainty in resistivity measurements.

5 Conclusion and Perspectives

This study presents an approximation method for evaluating the geometric factor in both unreinforced and reinforced geometries. It demonstrates that surrogate models, such as neural networks, can effectively approximate the geometric factor with high accuracy. To develop these models, a dataset was first generated using finite element modelling, performed with the open-access software Gmsh in combination with Matlab. Two different cases were considered: a homogeneous cuboid specimen and a cuboid specimen reinforced at the center with a single steel bar. In both cases, the surrogate models provided highly accurate predictions of the geometric factor. Their validity was confirmed by comparison with existing literature, particularly the studies by Minagawa et al. (2023) [1] and Presuel-Moreno et al. (2013) [2]. Additionally, an illustration of the geometric factor variations in both reinforced and non-reinforced prismatic specimens highlights the importance of evaluating this factor at any location within the investigated domain, especially when studying the spatial variability of resistivity.

Future work should focus on extending this approach to develop new approximation models for other reinforced and non-reinforced geometries, such as cylinders, columns and slabs, to further generalize the methodology. Additionally, demonstrating the applicability of this approach for on-site measurements would enhance its practical relevance. Another key advancement would be the development of a graphical user interface (GUI) that allows inspectors to rapidly evaluate the geometric factor for any desired geometry without the need to create a finite element model for each specific case and measurement position.

In conclusion, this study provides a generalized method for evaluating the geometric factor across various shapes, marking a significant milestone in accelerating the processing of measured resistivity data and facilitating spatial variability analysis.

References

1. H. Minagawa, S. Miyamoto, I. Kurashige, M. Hisada, Appropriate geometrical factors for four-probe method to evaluate electrical resistivity of concrete specimens. Construction and Building Materials. **374**, 130784 (2023)
2. F. Presuel-Moreno, Y. Liu, Y.-Y. Wu, Numerical modeling of the effects of rebar presence and/or multilayered concrete resistivity on the apparent resistivity measured via the Wenner method. Construction and Building Materials. **48**, 16 (2013)
3. R. B. Polder, Test methods for on site measurement of resistivity of concrete Ђ a RILEM TC-154 technical recommendation, (2001)
4. H. W. Whittington, J. McCarter, M. C. Forde, The conduction of electricity through concrete. Magazine of Concrete Research. **33**, 48 (1981)
5. M.-A. Eid, N. Reuge, G. Villain, S. Bonnet, S. P. Lopes, Monitoring of drying and imbibition of concrete using embedded resistivity sensors for the estimation of permeability. Cement and Concrete Composites. **157**, 105900 (2025)
6. M. Saleem, M. Shameem, S. E. Hussain, M. Maslehuddin, Effect of moisture, chloride and sulphate contamination on the electrical resistivity of Portland cement concrete. Construction and Building Materials. **10**, 209 (1996)
7. N. S. Piro, A. S. Mohammed, S. M. Hamad, Electrical resistivity measurement, piezoresistivity behavior and compressive strength of concrete: A comprehensive review. Materials Today Communications. **36**, 106573 (2023)
8. J. F. Lataste, C. Sirieix, D. Breysse, M. Frappa, Electrical resistivity measurement applied to cracking assessment on reinforced concrete structures in civil engineering. NDT & E International. **36**, 383 (2003)
9. H.-W. Song, V. Saraswathy, Corrosion Monitoring of Reinforced Concrete Structures – A Review. International Journal of Electrochemical Science. **2**, 1 (2007)
10. H. Layssi, P. Ghods, A. R. Alizadeh, M. Salehi, Electrical Resistivity of Concrete. (n.d.)
11. W. Morris, E. I. Moreno, and A. A. Sagüés, Practical evaluation of resistivity of concrete in test cylinders using a Wenner array probe. Cement and Concrete Research. **26**, 1779 (1996)
12. M. A. Alhajj, S. Palma-Lopes, G. Villain, Accounting for steel rebar effect on resistivity profiles in view of reinforced concrete structure survey. Construction and Building Materials. **223**, 898 (2019)
13. K. Reichling, M. Raupach, N. Klitzsch, Determination of the distribution of electrical resistivity in reinforced concrete structures using electrical resistivity tomography. Materials & Corrosion. **66**, 763 (2015)

14. L. Yang, D. Yang, Q. Yuan, Electrical resistivity tomography through reinforced concrete floor. Near Surface Geophysics. **22**, 47 (2024)
15. A. Q. Nguyen, G. Klysz, F. Deby, J.-P. Balayssac, Evaluation of water content gradient using a new configuration of linear array four-point probe for electrical resistivity measurement. Cement and Concrete Composites. **83**, 308 (2017)
16. A. J. Garzon, J. Sanchez, C. Andrade, N. Rebolledo, E. Menéndez, J. Fullea, Modification of four point method to measure the concrete electrical resistivity in presence of reinforcing bars. Cement and Concrete Composites. **53**, 249 (2014)
17. M. G. Sohail, S. Laurens, F. Deby, J. P. Balayssac, Significance of macrocell corrosion of reinforcing steel in partially carbonated concrete: numerical and experimental investigation. Mater. Struct. **48**, 217 (2015)
18. A. Nasser, A. Clément, S. Laurens, A. Castel, Influence of steel–concrete interface condition on galvanic corrosion currents in carbonated concrete. Corrosion Science. **52**, 2878 (2010)
19. G. Samson, F. Deby, J.-L. Garciaz, J.-L. Perrin, A new methodology for concrete resistivity assessment using the instantaneous polarization response of its metal reinforcement framework. Construction and Building Materials. **187**, 531 (2018)
20. P. Azarsa, R. Gupta, Electrical Resistivity of Concrete for Durability Evaluation: A Review. Advances in Materials Science and Engineering. **2017**, 1 (2017)
21. M. K. El Achrafi, G. Villain, S. Bonnet, Surface calibration of electromagnetic properties to simultaneously consider water and chloride contents in concrete both with and without slag. Construction and Building Materials. **417**, 135176 (2024)
22. P. Ghosh, Q. Tran, Correlation Between Bulk and Surface Resistivity of Concrete. Int. J. Concr. Struct. Mater. **9**, 119 (2015)
23. Y. Lecieux, F. Schoefs, S. Bonnet, T. Lecieux, S. P. Lopes, Quantification and uncertainty analysis of a structural monitoring device: detection of chloride in concrete using DC electrical resistivity measurement. Nondestructive Testing and Evaluation. **30**, 216 (2015)
24. M. K. El Achrafi, S. Bonnet, G. Villain, Electrical resistivity tomography results analyzed with two inversion methods to determine chloride profiles on BFS concrete having very high electrical resistivity. Construction and Building Materials. **407**, 133361 (2023)
25. A. White, J. Boyd, P. Wilkinson, H. E. Unwin, J. Wookey, J. M. Kendall, A. Binley, J. Chambers, Assessing the effect of offline topography on electrical resistivity measurements: insights from flood embankments. Geophysical Journal International. **239**, 1117 (2024)
26. L. Marescot, S. Rigobert, S. Palma Lopes, R. Lagabrielle, D. Chapellier, A general approach for DC apparent resistivity evaluation on arbitrarily shaped 3D structures. Journal of Applied Geophysics. **60**, 1 (2006)
27. C. Geuzaine, J.-F. Remacle, Gmsh: a three-dimensional finite element mesh generator with built-in pre- and post processing facilities. International Journal for Numerical Methods in Engineering. **79**, 1309 (2009)
28. S. M. Harle, Advancements and challenges in the application of artificial intelligence in civil engineering: a comprehensive review. Asian J. Civ. Eng. **25**, 1061 (2024)